# Fate of cohesive sediments in a marsh-dominated estuary

Xiaohe Zhang[1*], Nicoletta Leonardi[2], Carmine Donatelli[2], Sergio Fagherazzi[1]

[1]Department of Earth and Environment, Boston University, Boston, Massachusetts, USA

[2]Department of Geography and Planning, University of Liverpool, UK

zhangbu@bu.edu

**Abstract**

Deposition of fine sediments on a marsh platform favors accretion that counteracts Sea Level Rise. However, it is difficult to assess the sediment trapping capacity of a marsh given the heterogeneity of sediment sources and the geometric complexity of the system, with a network of dendritic and meandering creeks dissecting the intertidal area. Here we use a numerical model to study the sediment trapping capacity of a marsh-dominated estuary, Plum Island Sound, USA, and its variations across the landscape. The results highlight the importance of the timing between sediment inputs and tidal phase and show that sediment discharged from tidal rivers deposit within the rivers themselves or in adjacent marshes. Most sediment is deposited in shallow tidal flats and channels and is unable to penetrate farther inside the marshes because of the limited water depths and velocities on the marsh platform. Trapping capacity of sediment in different intertidal subdomains decreases logarithmically with the ratio between advection length and the typical length of channels and tidal flats. Moreover, sediment deposition on the marsh decreases exponentially with distance from the channels and marsh edge. This decay rate is a function of settling velocity and the maximum value of water depth and velocity on the marsh platform.

**Keywords:** salt marshes, numerical modelling, sediment exchange, trapping capacity, ponds expansion

## 1. Introduction

Salt marshes are among the most valuable coastal landforms in the world, supporting productive ecosystems and buffering the shoreline against violent storms. In recent years, salt marshes have experienced increasing pressure from Sea Level Rise (SLR) and human activities (e.g. a decrease in riverine sediment supply due to dams) [*Syvitski et al.,* 2005, 2007; *Dai et al.,* 2014; *Dai and Liu*., 2013; *Craft et al*., 2009]. Marsh drowning due to SLR and wave induced horizontal retreat has been well documented around the world [*Fagherazzi et al.*, 2013; *Kirwan and Murray*, 2007; *Leonardi and Fagherazzi*, 2014; *Leonardi et al*., 2017]. *Fagherazzi et al*., [2013] and *Ganju et al.*, [2017]

highlight the critical role that sediment supply and sediment transport mechanisms play in the resilience of salt marshes against SLR and human perturbations. *Kirwan et al*., [2016] used process-based models based on biophysical feedbacks to predict the threshold rate of SLR for marsh survival. Their results indicate that marshes can survive under relatively high SLR rates only if abundant sediment is available. *Ganju et al*., [2015] found that a marsh can laterally erode despite having high SSC and accretion rates. They suggested the flood/ebb SSC ratio as a better vulnerability metric, since it mimics the difference between the sediment entering and exiting the marsh complex. Another vulnerability metric is the ratio between unvegetated and vegetated areas, which well predicts the sediment deficit of microtidal marsh systems [*Ganju et al*., 2017]. All these recent results indicate that sediment fluxes are critical in determining marsh vulnerability to SLR.

The possible sources of sediments vary in different systems, and most coastal bays may lack riverine sediment inputs. In a recent work, *Hopkinson et al.,* [2018] evaluated the sediment budget of Plum Island Sound by comparing LiDAR data taken in different years. They found that marsh edge erosion provides more 30% of the sediment required to counteract SLR, whereas riverine sediments provide less than 10 %. This indicates that sediment fluxes from the ocean and from tidal flats should account for more than 50% of the budget. It is thus critical to understand the fate of suspended sediments in a salt marsh complex, and the trapping capacity of different marsh locations with respect to potential sources of sediments, including rivers, bays and the coastal ocean. Understanding the source and fate of sediments within marshes is of paramount importance in determining the future resilience of these ecosystems.

Marshes are able to capture fine cohesive sediments, because the thick vegetation reduces flow speed and turbulence allowing the deposition of small particles [*Fagherazzi et al.*, 2012; *Mehta*, 2014]. However, it is difficult to quantify sediment transport dynamics in an estuary due to the complex geometry of the intertidal landscape, with dendritic channel networks dissecting salt marshes [*Fagherazzi et al*., 1999]. Numerical simulations provide the opportunity to explore sediment trajectories in such a complex environment. For example, simulations can capture the residence time of sediment particles and tracers in intertidal areas [*Defne et al.*, 2016; *Mercier and Delhez*, 2007] and tidal rivers [*Ralston and Geyer*, 2017].

Point field measurements have identified that increasing elevation, distance to channels and marsh edges, and flow friction due to vegetation canopy affect the spatial distribution of sediment deposition rates on marshes

[*Christiansen et al.*, 2000; *Fagherazzi et al.*, 2012; *Reed et al.*, 1999; *Temmerman et al.*, 2005a]. *Temmerman et al.*, [2003] proposed an empirical model by relating sedimentation to platform surface elevation, distance to nearest channel or marsh edge, and distance to marsh edge measured along the nearest creek. The model well captured spatial variations of sedimentation over the marsh platform in the Scheldt estuary (Belgium, SW Netherlands).

A simplified advection-dispersion equation of suspended sediment transport over marshes indicates that settling velocity, inundation depth, and flow velocity determine the decay rate of sediment concentration along a transect perpendicular to the creek bank or marsh edge [*Fagherazzi et al.*, 2012], but it is not clear whether this simplified model can be applied to a natural system with a complex channel network. Flow velocities over the marsh platform are relatively small compared to those in the channels, and significantly vary in space and time during a tidal cycle. For example, the peak velocity is one order of magnitude larger than the velocity during high slack water [*Leonard and Luther*, 1995]. As a result it is difficult to determine what hydrodynamic conditions are responsible for the advection of sediment in the marsh.

The role of vegetation in sediment transport dynamics is well captured in recent numerical models. The effect of vegetation structures on momentum, turbulence, and water exchange dynamics [*Nepf and Vivoni*, 2000] is solved in the hydrodynamic models Delft3D [*Baptist*, 2005; *Temmerman et al.*, 2005b] and ROMS [*Tarandeep et al.*, 2017]. 2D and 3D hydrodynamic models have produced excellent results in a variety of vegetated coastal environments, ranging from deltaic wetlands [*Nardin and Edmonds*, 2014; *Donatelli et al*., 2018] to mangrove forests [*Horstman et al.*, 2015]. Among these studies, it was found that vegetation with intermediate height and density enhances sedimentation in river deltas such as the Wax Lake Delta, USA [*Nardin and Edmonds*, 2014]. *Horstman et al.*, [2015] highlighted the sensitivity of tropical shorelines to coupled sediment-vegetation dynamics by showing a significant decrease in sediment trapping efficiency driven by loss of mangroves and a reduction in sediment inputs. Moreover, by including vegetation growth and mortality, *Oorschot et al.*, [2016] showed that a dynamic vegetation provides more realistic results in the long-term evolution of mangrove shorelines. *Donatelli et al*., [2018] used the newly developed vegetation model in ROMS to investigate the impact of seagrass beds on sediment transport dynamics. They found that the presence of seagrasses increases the total sediment budget of coastal embayment but reduces the amount of sediment in suspension and delivered to marsh platforms during high tide.

82 The vegetation module of the model Delft3D was tested in *Temmerman et al.*, [2005b]. In this model the momentum
83 drag and turbulence structure induced by the vegetation are solved numerically using the k-ε turbulence closure.
84 Sensitive analyses show that a 2D vegetation model can also be used to reduce computational cost, without a
85 significant loss in accuracy despite the absence of three-dimensional turbulence [*Horstman et al.*, 2013]. In this
86 manuscript, we have applied the 2D Delft3D FLOW/MOR model with the vegetation module to Plum Island Sound,
87 Massachusetts, USA, a mesotidal bay dominated by salt marshes (Fig. 1). The bay hosts the Plum Island Ecosystems
88 of Long-Term Ecological Research program (PIE-LTER).

89 The goal of this work is to determine the fate of cohesive sediments in the system. Specifically, we will explore the
90 sediment trapping capacity of different marsh subdomains by releasing sediments at different locations, at different
91 instants within the tidal cycle, and with sediment grain sizes ranging from clay to silt. Furthermore, characteristic
92 scales of sediment deposition and factors controlling suspended sediment transport over the marsh platform are
93 analyzed in order to clarify the mechanisms.

94

95 ## 2. Methods

96 ### 2.1 Study area

97

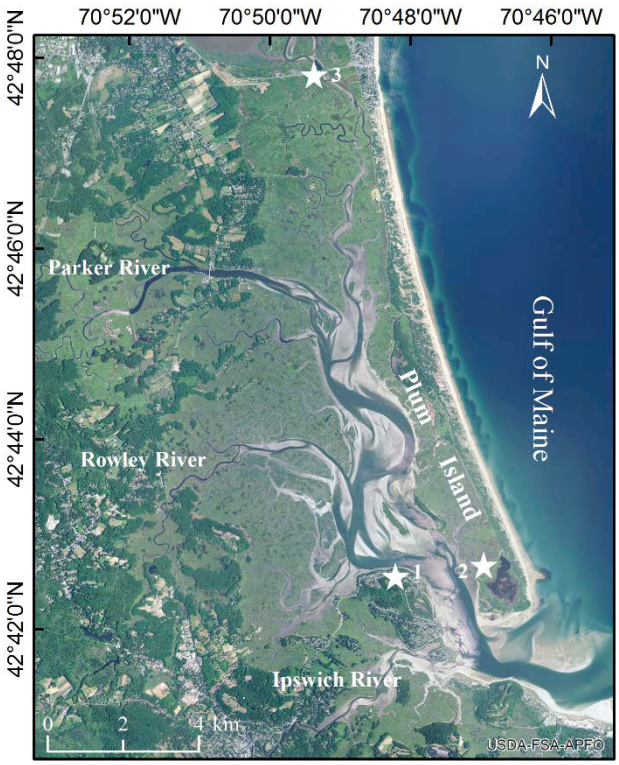


Figure 1. Aerial photograph of Plum Island Sound (0.6 m resolution map provided by the National Agricultural Imagery Program from US Department of Agricultural). The location of tidal stations (stars) are indicated; tidal station 1 is at Ipswich Bay Yacht Club pier and belongs to PIE-LTER, station 2 is a NOAA station (8441241), and station 3 is the USGS gauge (424752070491701) at TPK BRIDGE.

Plum Island Sound (Fig.1) is a coastal plain, bar-built estuary with extensive areas of productive tidal marshes dominated by *Spartina alterniflora* and *Spartina patens.* The estuary is located along the northeastern Massachusetts shoreline, and is fed by the Ipswich, Rowley and Parker Rivers. The tide is semi-diurnal with a mean range of 2.6 m. An inlet connects the sound to the Atlantic Ocean [*Fagherazzi et al.*, 2014; *Zhao et al.*, 2010]. Because of the relatively high tidal energy, the tide induced bed shear stresses are larger than the wind-wave stresses, except during extreme storms [*Fagherazzi et al.*, 2014].

The bathymetry of the estuary is characterized by extensive tidal flats and a deep (more than 5 m) central channel [*Fagherazzi et al.*, 2014]. We define marsh the area between 0.09 m (mean sea level in NAVD88) and 1.453 m (MHHW); upland the area higher than 1.453 m [*Wilson et al.*, 2014]. Marshes account for 60% of the estuary surface (Fig.2a). In addition, in order to determine the exchange of sediment across different parts of the estuary, the

system is divided in eight subdomains named: Upper Estuary, Parker River, Rowley River, Ipswich River, Upper Sound, Lower Sound, Inlet, and Ocean (Fig.2b).

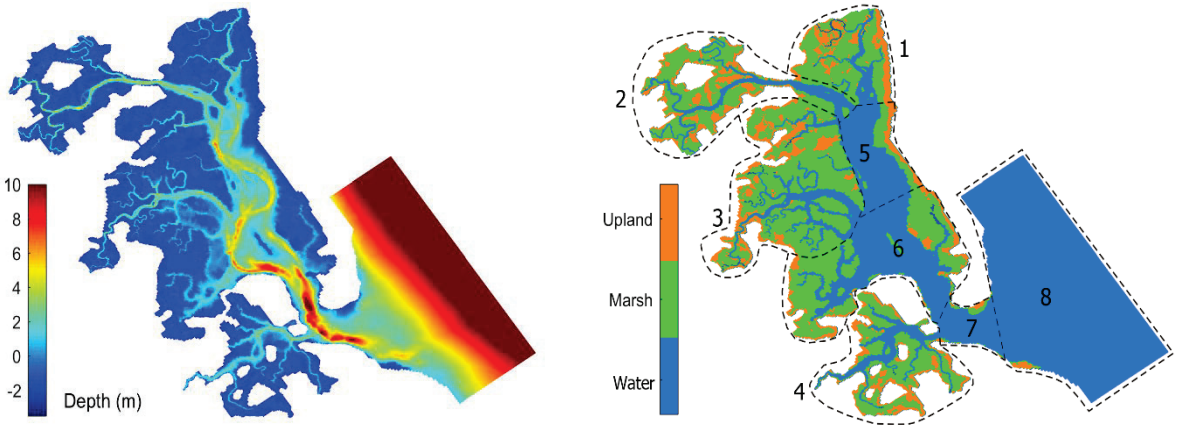


Figure 2. Plum Island Sound bathymetry (left) and subdivision in upland, marsh, and ocean areas based on depth (right); 1-8 are subdomains marked by dash lines: 1) Upper Estuary, 2) Parker River, 3) Rowley River, 4) Ipswich River, 5) Upper Sound, 6) Lower Sound, 7) Inlet, 8) Ocean.

**2.2 Numerical model setup**

We use the Delft3D model coupled to the 2DH vegetation module to simulate tidal flow and the transport of cohesive sediments. The domain consists of 703×410 cells with a resolution of 20×20 m (Fig. 2). Tidal harmonic constituents (M2, S2, N2, K1, M4, O1) at the NOAA station 8441241 (see location 2 in Fig. 1) are prescribed at three ocean boundaries at the beginning of the simulations. The phases of harmonic constituents are modified to match the water level data at the Ipswich Bay Yacht Club pier (see location 1 in Fig. 1).

The daily averaged flow discharge data of the Parker (1 $m^3/s$) and Ipswich Rivers (5 $m^3/s$) are available at USGS gauges (01101000, 01102000), while that of Rowley River (0.2 $m^3/s$) is obtained by scaling the Ipswich River discharge to the watershed area [*Fagherazzi et al.*, 2014; *Zhao et al.*, 2010]. Although previous work highlights the contribution of saline water from Plum Island Sound to the Merrimack River, the yearly daily averaged flow discharge recorded at the USGS gauge (424752070491701) TPK BRIDGE (see location 3 in Fig. 1) is 3.7 $m^3/s$, being ignorable compared to tidal prism ($6.37\times10^7$ $m^3$) of entire domain. The water only outflows from Plum Island Sound to the Merrimack River during relatively low water levels.

For the bed roughness we set the following Chezy coefficients: 45 $m^{1/2}s^{-1}$ for the ocean, rivers and main tidal channels, 40 $m^{1/2}$ $s^{-1}$ for the tidal creeks, and 35 $m^{1/2}$ $s^{-1}$ for the marsh platform. The 2DH vegetation module uses the directed point model DPM, and the vegetation drag effects on the momentum equations are solved based on *Baptist* [2005]. Specifically, a term $-\frac{1}{2}\lambda u_v^2$ is included within the momentum equation to account for the flow resistance due to vegetation, where $\lambda$ is a flow resistance coefficient and $u_v$ is the flow velocity [*Nepf and Vivoni*, 2000; *Yang et al.*, 2015]. For the emergent vegetation case with $h < h_v$, the net bed roughness and flow resistance are $C = C_b, \lambda = C_D n$, where $h$ is water depth, $h_v$ is vegetation height, $C$ is net bed roughness including vegetation effect, $C_b$ is bed roughness without vegetation, and $n$ is vegetation density. For the submerged vegetation case with $h > h_v$, the net bed roughness and flow resistance coefficient are:

$$C = C_b + \frac{\sqrt{g}}{\kappa}\ln\left(\frac{h}{h_v}\right)\sqrt{1 + (2g)^{-1}C_D n h_v C_b^2} \quad (1)$$

$$\lambda = C_D n \frac{h_v}{h}\frac{C_b^2}{C^2} \quad (2)$$

Where $g$ is gravity acceleration, $\kappa$ is Kármán's constant equal to 0.4. We define uniform and representative vegetation parameters for the marsh area based on *Johnson et al.*, [2016]: $h_v$=0.4m, stem diameter *D*=3.5 mm, stem density *n*=1200 stems /$m^2$, $C_D$=1.

Two main fractions of cohesive sediments are tested based on field observations, namely a coarse silt with grain size 32-64 μm and settling velocity of 3.6 mm $s^{-1}$ and a clay fraction with grain size less than 32 μm with a settling velocity of 0.5 mm $s^{-1}$ [*Wiberg et al.*, 2015]. Erosion (E) and deposition (D) of cohesive sediments in Delft3D are calculated with the Partheniades-Krone equations [*Partheniades,* 1965]:

$$E = M\left(\frac{\tau}{\tau_e} - 1\right), \tau > \tau_e \quad (3)$$

$$D = w_s C \quad (4)$$

Where τ is bed shear stress, $\tau_e$ is the critical bed shear stress for erosion, *M* is an empirical erosion parameter, and $w_s$ is the setting velocity of suspended cohesive sediments. We adopt the same parameters used in Delft3D simulations for the Virginia Coast Reserve, a similar system of intertidal bays along the Eastern Shore of Virginia [*Wiberg et al.*, 2015]. $\tau_e$ is set to 0.05 N $m^{-2}$, *M* to $1\times10^{-5}$ kg $m^{-2}$ $s^{-1}$ and the dry bed density to 795 kg $m^{-3}$. Note that in this study we are not considering the possible coarser material (sand) present at the channel bottoms, but only the fine material that is exchanged between channels and salt marsh platform.

From 1994 to 2015, water samples along the Plum Island estuary from the Parker River Dam to the mouth of the sound were collected within 2 hours of either high tide or low tide in the spring and fall seasons. The median value of 13-year suspended sediment concentration along the transect peaks approximately at 40 mg/L at the mouth of the Parker River, decreases in the sound, and reaches a lower value of 15 mg/L at the inlet. Generally, the concentration is higher in the spring when river discharge is high [*Hopkinson et al.,* 2018]. An initial suspended sediment concentration of 30 mg/l was released in different subdomains at different instants of the tidal cycle. The bottom elevation was maintained fixed during the simulations. To maintain model stability even with parallel computing, we set the time step to be 0.3 minutes.

**2.3 Numerical Simulations**

We release a depth-averaged suspended sediment concentration of 30 mg/l in the water area of the subdomains 1 to 7 (see Fig.2). The suspended sediment was released at four different instants during a spring tidal cycle: at high water level (SH), mean water level during ebb (ME), low water level (SL) and mean water level during flood (MF). The physical parameters of the cohesive sediment were kept uniform with a settling velocity of 0.5 mm $s^{-1}$, and a critical shear stress for erosion of 0.05 N $m^{-2}$. Since in all scenarios the suspended sediment mass in the water column after 1 month is negligible, we only measured the sediment mass deposited at the bottom of the different subdomains.

To determine the role of different intertidal geometries on sediment transport dynamics we choose the Rowley River as a representative marsh-dominated area and the Upper Sound as an intertidal area with limited marsh. We determine the distribution of deposited cohesive sediments after one month as a function of water depth in three landforms: salt marshes (elevation between 0.09 and 2m), tidal flats (elevation between 0.09 and -2m), and deep channels (elevation below -2). For every marsh cell, we calculate the minimum distance to the tidal flats/channels, as well as the averaged values of both maximum and mean flow velocity and inundation depth during marsh flooding.

**2.4 Characteristic scales of sediment deposition**

188 The dynamics of sediment deposition is controlled by advection of sediment and settling. Advection depends on the
189 average velocity of the tidal flow $U$ while settling depends on water depth $h$ and settling velocity $\omega_s$. We define a
190 sediment transport length $L_0$ as the distance a sediment particle travels before depositing:

191 $$L_0 = \frac{Uh}{\omega_s} \quad (5)$$

192 We define the non-dimensional parameter $R$ as the ratio between the sediment transport length $L_0$ and the
193 characteristic spatial dimension of a reference area $L$:

194 $$R = \frac{L_0}{L} \quad (6)$$

195 If $R$>1, the sediment is likely to leave the reference area, while if $R$<1 the sediment is trapped in it. The values of the
196 dimensional scales are reported in Table 1 for all the subdomains of the estuary (Fig.2b).

197 Following *Fagherazzi et al.* [2012], we examine the deposition rate on the marsh platform using the advection
198 equation:

199 $$\mathrm{C} = \mathrm{C}_0 \exp(-\mathrm{x}/L_m) \quad (7)$$

200

201 Where C is the suspended sediment concentration along a transect perpendicular to the marsh boundary (kg/m$^3$), $C_0$
202 is the concentration at the boundary between marsh and channel/tidal flat, $L_m = U_m h_m/\omega_s$ is the sediment transport
203 length on the marsh, $U_m$ and $h_m$ are the average velocity (m/s) and water depth (m) on the marsh platform during
204 flooding, x is distance from the marsh edge (m). The deposition rate is computed as the divergence of the sediment
205 flux:

206 $$D = -\frac{\mathrm{d}(CU_m h_m)}{\mathrm{dx}} = C\omega_s \exp(-\mathrm{x}/L_m) \quad (8)$$

207 Where $D$ indicates deposition rate (kg/m$^2$/s).

208 Equation 7 and 8 are evaluated for the entire marsh area, computing the distance from the edge of each marsh point
209 and utilizing the average value of velocity and water depth on the marsh platform computed with Delft3D.

210 Table 1. Dimensional scales for the seven subdomains. Values are calculated only in water areas as showed in Fig.2.

| Location | Order | h (m) | L (m) | $\omega_s$ (mm/s) | U (m/s) | $L_0$ (m) | $R=L_0/L$ |
|---|---|---|---|---|---|---|---|

| | | | | | | | |
|---|---|---|---|---|---|---|---|
| Upper Estuary | 1 | 1.84 | 3262 | 0.5 | 0.14 | 513.72 | 0.16 |
| Parker River | 2 | 2.55 | 7836 | 0.5 | 0.24 | 1217.46 | 0.16 |
| Rowley | 3 | 1.72 | 5727 | 0.5 | 0.19 | 636.81 | 0.11 |
| Ipswich | 4 | 1.48 | 4441 | 0.5 | 0.20 | 602.21 | 0.14 |
| Upper Sound | 5 | 2.42 | 3001 | 0.5 | 0.27 | 1297.09 | 0.43 |
| Lower Sound | 6 | 2.95 | 3761 | 0.5 | 0.39 | 2324.25 | 0.62 |
| Inlet | 7 | 3.60 | 1507 | 0.5 | 0.69 | 4975.34 | 3.30 |

## 3. Results

### 3.1 Sediment trapping capacity

A dependency matrix shows the distribution of trapped sediment across the estuary (Fig.3). The diagonal elements indicate the fraction of sediment that deposits in the same subdomain where it was released. The off-diagonal elements record the sediment deposited in a subdomain different from the one of the initial release. In the Upper Estuary, Parker River, Rowley River, and Ipswich River most sediments are deposited in the release area irrespectively of the timing of release. In the Lower Sound and Inlet domains, the strong tidal currents resuspend and transport the cohesive sediments to low energy areas. Generally, a large fraction of the sediments released in the rivers is kept in the estuary, with an exception of the Ipswich River because of its proximity to the inlet and the strong currents in the lower part of the sound.

The differences among the four matrixes reported in Fig.3 highlight the role of the timing of release in the sediment trapping efficiency within the estuary. The trapping efficiency is high in the MF case (mean water level during flood), since more sediment is transported landward during flood and then deposits in low energy areas. On the contrary, if released during ebb (ME), more sediment is flushed out of the system.

As expected, a large fraction of the sediment is exchanged between the Upper and Lower Sound, and more sediment deposits in the Upper Sound when released in the Lower Sound during flood. The direct sediment exchange among the four marsh-dominated subdomains (the Upper Estuary, Parker River, Rowley River, and Ipswich River) is very limited and only occurs through the sound. No cohesive sediment released at the inlet remains there but it is either discharged to the ocean or trapped in the tidal reaches and marshes of the Rowley and Ipswich Rivers. Hardly any sediment released at the inlet reaches the Parker River and Upper Estuary, even in the flood scenario.

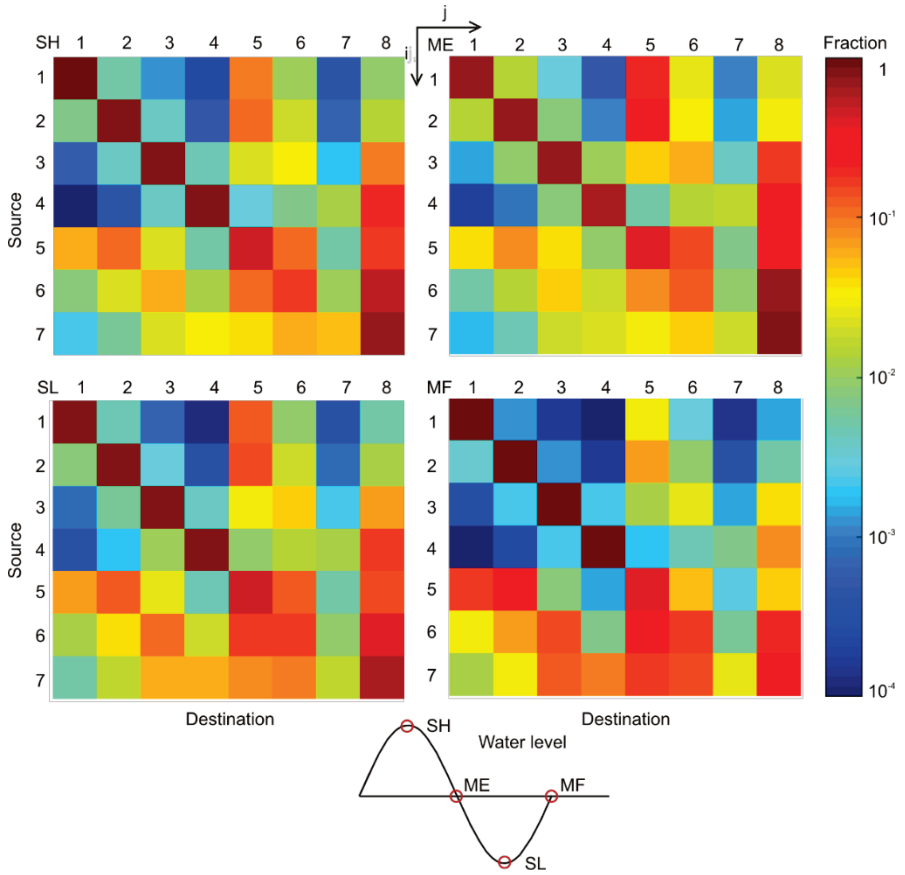


Figure 3. Dependency matrix of sediment deposition in Plum Island Sound after 30 days. Values (i,j) in the table indicate the mass fraction of sediments released in region i (source) and captured within region j (destination). The subdomains are: 1) Upper Estuary, 2) Parker River, 3) Rowley River, 4) Ipswich River, 5) Upper Sound, 6) Lower Sound, 7) Inlet, 8) Ocean.

### 3.2 Sediment exchange processes and mechanisms

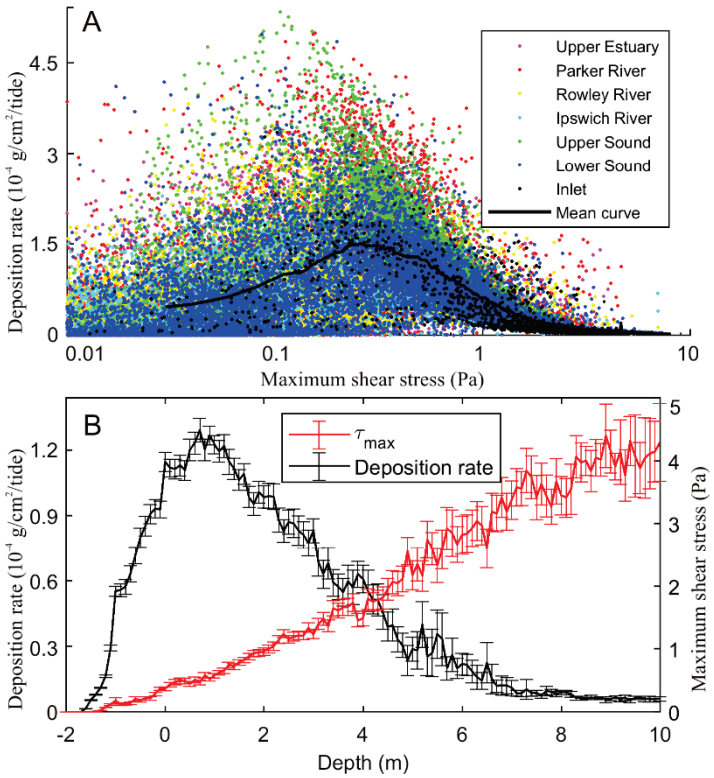


Figure 4. (A) Distribution of deposition rate as a function of maximum shear stress during a spring tidal cycle in seven subdomains; mean curve is binned in intervals of 0.01 Pa. (B) Distribution of maximum shear stress and deposition rate as a function of water depth; data are binned in intervals of 0.2 m with confidence interval of 95%.

We then explore whether sediments are preferentially deposited in quiet areas experiencing low tidal velocities and low bottom shear stresses. High tidal flow can in fact resuspend sediments and move them in areas where the velocity is lower (for example in salt marshes and shallow tidal flats). Our results show that this is not always the case (Fig. 4A) and the sediments are prevalently deposited in areas experiencing intermediate bottom shear stresses. Similarly, sediments are mostly deposited at water depth between 0 and 2 meters, typical of tidal flats and tidal bars and not at water depths above mean sea level, typical of salt marshes (Fig. 4B). The results of Fig.4B are in agreements with the results of Fig.4A, since tidal bars and flats experience intermediate bottom shear stresses, while marshes are characterized by very low shear stresses. These results indicate that sediment availability and sediment pathways are also important, and that only a small fraction of sediment is reaching the marsh platform. This is partly due to the fact that at time zero the sediments are not released on the marsh platform, but only in areas covered with water at mean sea level (tidal channels and tidal flats, the likely sources of sediment). Yet the fact that a small fraction of sediment reaches the marsh platform seems counterintuitive and it is an important result.

Within the Rowley River area, clay ($\omega_s$ = 0.5 mm/s) is mostly deposited in the marshes and tidal flats. Deposition of coarse silt ($\omega_s$ = 3.6 mm/s) follows the same distribution with a slight shift toward lower areas. In the Upper Sound, a larger fraction of both mud and coarse silt is transferred into deep channels with less sediment deposited on the marshes (Fig. 5). We also find that the distribution of deposited sediments is controlled more by the physical attributes of each area (i.e. presence of salt marshes), rather than by the grain size and settling velocity.

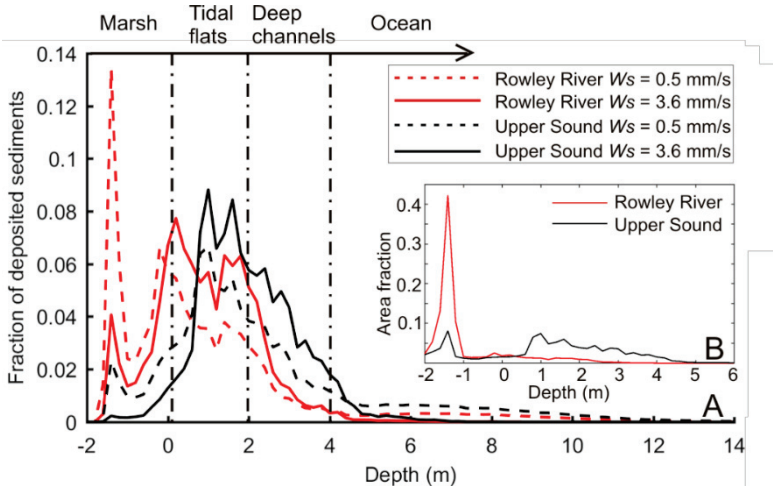


Figure 5. (A) Distribution of deposited sediments as a function of water depth in four different scenarios: clay ($\omega_s$=0.5 mm/s) and coarse silt ($\omega_s$=3.6 mm/s) released in the Rowley River and Upper Sound. (B) Distribution of area as a function of water depth for Rowley River and Upper Sound. Note the data are binned in intervals of 0.2 m.

The distributions of deposited sediment as a function of water depth display peaks in the marsh area (elevations around 1.3 m) and in the tidal flats, which correspond to the larger area fractions showed in Fig. 5B. High values of bottom shear stress hinder the deposition of cohesive sediment in the rivers and large tidal channels. As a result, sediments that reach these channels are transported to either shallow areas or to the ocean. Sediment released in the Rowley River is deposited mostly in tidal flats and salt marshes, while a smaller fraction is deposited in the tidal channels or exported to the ocean (Fig. 6a). In time the volume of sediments deposited on the marsh increases, collecting sediments resuspended in tidal flats and channels. Note that the amount of sediments gained by marshes is higher than the sediment lost by tidal flats, indicating that channels actively feed the marsh surface. Channels also contribute to the export of sediment to the ocean. Overall, most sediments are deposited within hours after the release and moderate variations occur because of resuspension.

Because tidal flats and deep channels have a similar area in the Upper Sound, at the beginning of the simulation an equal amount of mud is deposited on these two landforms (Fig. 6b). Similarly to the Rowley River case, the sediment deposited in the deep channels decreases while it increases on the marshes and tidal flats over time, and some of these sediments are also exported to the ocean. In the Upper Sound, changes in the sediment reservoirs are larger in time, with marshes increasing the trapped sediments twofold and the sediments stored in the channels decreasing of 40%. We ascribe these larger variations to intense tidal flows that remobilize bottom sediments. Interestingly, the total amount of sediments stored in tidal flats increases in time. This is likely due to the larger extent of the flats area in the Upper Sound. Some of these tidal flats provide the quiet environment for permanent sediment settling. On the contrary, tidal flats are almost absent in the Rowley River, where tidal bars at the side and center of the river represent the most conspicuous landform between MSL and 2 m of depth. Because of the proximity to the river, the tidal flow on these bars is strong, easily remobilizing the deposited sediment.

The rivers and deep channels are therefore dynamic transit areas that control sediment remobilization within the estuary, feeding the marshes or exporting sediment to the ocean. This is particularly true for estuaries and bays characterized by the presence of large tidal channels, as in our study site.

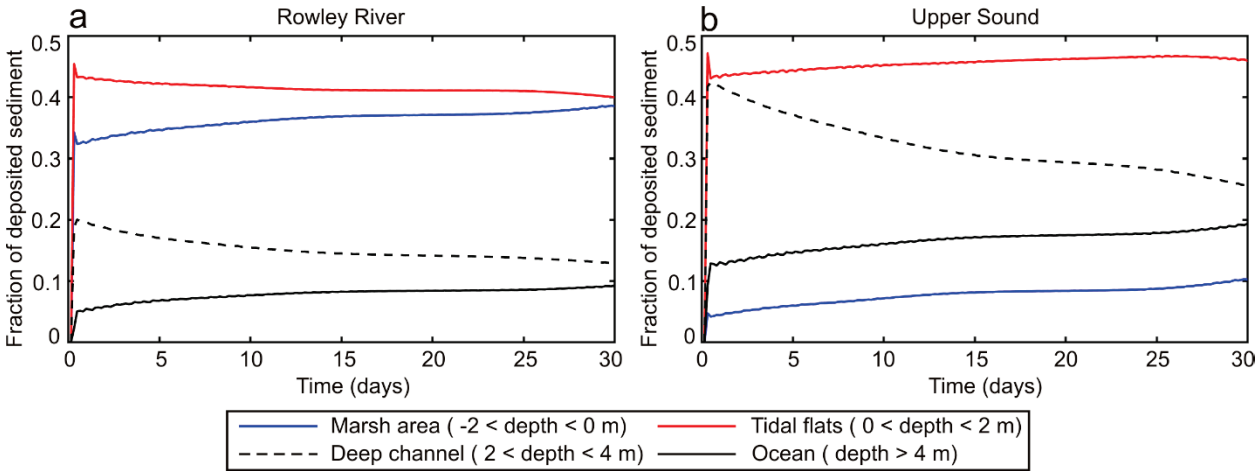


Figure 6. Temporal variations of deposited sediment within four different landforms (see legend), released in the Rowley River (a) and Upper Sound (b) with setting velocity $\omega_s$= 0.5 mm/s.

### 3.3 Factors controlling deposition on marshes and location of ponds

The mean values of velocity and water depth on the marsh surface computed with Delft3D during marsh submergence are $U_m = 0.015\ m/s$ and $h_m = 0.197\ m$, The sediment transport length $L_m$ on the marsh surface (Eq. 7) is 5.9 m while it becomes 43.5 m using the maximum values of velocity and water depth ($U_{max} = 0.05\ m/s$, $h_{max} = 0.44\ m$).

The maximum and mean flow velocity and inundation depth during marsh flooding are plotted as a function of distance to the marsh edge in Fig. 7A and Fig.7B. Both maximum and mean values decay with distance with flow velocities decreasing more significantly (~ 4 times) than inundation depths (~ 2 times). Using the maximum flow velocity and inundation depth, Fig.7C well captures the logarithmical decay rate of deposition with distance from the marsh edge; the sediment transport length on the marsh $L_m$=43.5 m agrees with the field measurements of *Temmerman et al.*, [2003], who reported a length of 41.7 m (decay coefficient of -0.024 $m^{-1}$).

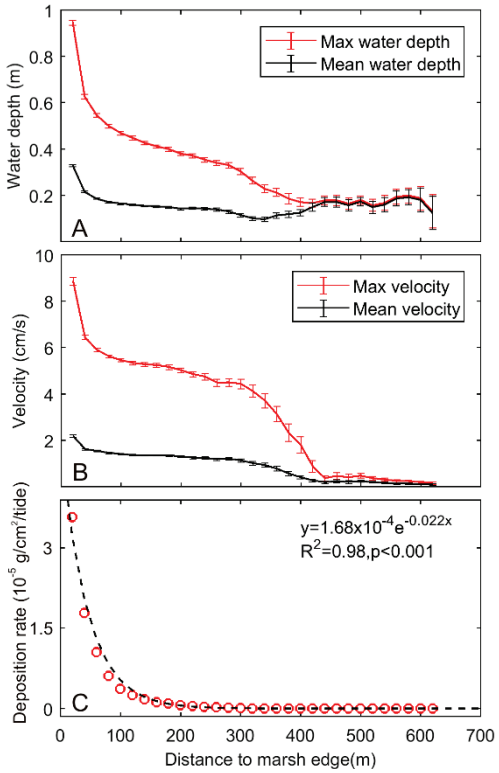


Figure 7. Maximum and mean values of water depth (A) and flow velocity (B) on the marshes during submergence as a function of distance to marsh edge; deposition rate (C) as a function of distance to marsh edge. The data are binned in intervals of 20 m with confidence of 95%.

On average, ponds/pools accounts for 4.5% of marsh platform from Virginia to Maine, USA [*Correll et al.,* 2018] and those present in the Plum Island marshes have expanded extensively in recent decades [*Wilson et al*., 2014].

Using 3-m resolution map of tidal marsh cover classes by random forest classifier with 90% overall map accuracy [*Correll et al.,* 2018], we calculated the distance of all ponds to the bay or closest channel for the entire Plum Island Sound (Fig. 8A). Histogram plot (Fig. 8B) of distances indicates that 40% of ponds area are located less than 50 m from channels, and 78% within a distance of 100 m. This is in agreement with the sediment transport length on the marsh $L_m$=43.5m and Fig.7C, showing that deposition is low farther than 100 m from channels.

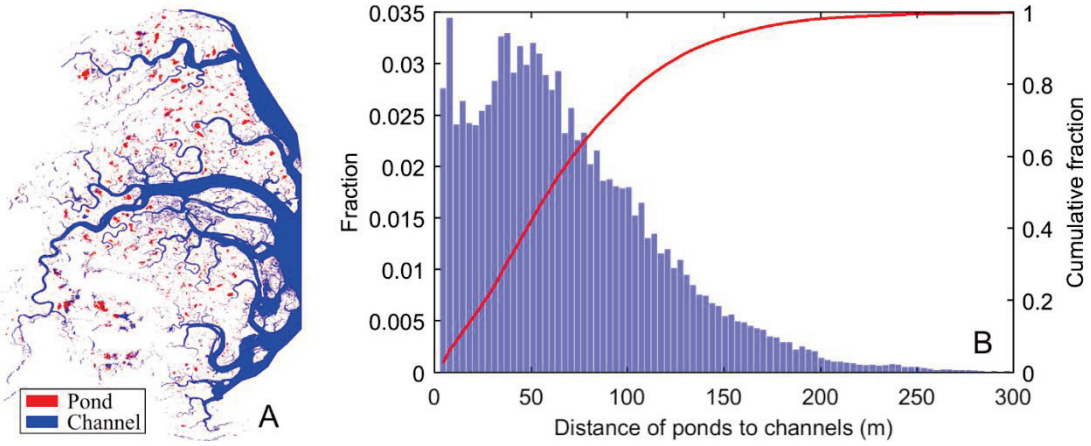


Figure 8. Locations of ponds and channels in the Rowley River derived by remote sensing classification map (A); (B) histogram of distance of ponds to channels for the entire Plum Island Sound (bar plots), and cumulative fraction (red line).

## 4. Discussion

Salt marshes are fed by sediments coming from rivers, sediments resuspended from tidal flats in the sound, and sediments fluxes from the ocean. A length ratio $R$ smaller than 1 (see table 1) indicates that most of the incoming cohesive sediment ($\omega_s \geq 0.5\ mm/s$) from the Parker, Rowley and Ipswich rivers can be hardly transported into the sound and is trapped in the rivers subdomains. Four marsh-dominated subdomains (the Upper Estuary, Parker River, Rowley River, and Ipswich River) can also receive sediment from the sound, and sediment coming from the ocean through the inlet can only feed the marshes bordering the Rowley and Ipswich Rivers. The Upper Estuary and Parker River can hardly receive sediment from the Ocean.

The timing between river floods, wind waves, and tidal stage affects sediment trapping. If the peak river discharge occurs during the flood phase of the tide, more riverine sediments will remain in the system. On the contrary, if the

334 peak discharge occurs during ebb, more sediment will be flushed to the ocean (Fig. 3). Similarly, sediment
335 resuspended during energetic wave events remain in the system during tidal food, but leave the system if the storm
336 occurs during ebb.

337 Hydrodynamics determine the trapping capacity of each subdomain. As showed in Fig.9, the trapping capacity of
338 sediment decreases exponentially with increasing non-dimensional parameter *R* in the different subdomains.
339 Therefore minor variations of *R* trigger large variations of sediment trapping capacity in the system. In Plum Island
340 Sound, the salt marshes are currently keeping pace with SLR at the expense of total marsh area via edge erosion
341 [*Wilson et al.,* 2014; *Hopkinson et al.,* 2018]. Bay enlargement together with SLR increase the tidal prism, leading to
342 higher water depths and higher tidal velocities within the channels, and thus increasing *R*. Tidal flats and channels in
343 the bay will therefore trap less sediment, flushing more material to the ocean. In the long term the flushing effect
344 will result in a net sediment loss for the entire system. On the other hand, higher water levels and velocities on the
345 marsh platform will also allow the sediment to be deposited further in the marsh [*Kirwan and Murray,* 2007;
346 *D'Alpaos et al.,*2007]. Moreover, less deposition in tidal flats and channels could be beneficial for the marshes, since
347 there will be more sediment in the water column to feed them. The feedback between SLR and sediment trapping
348 has therefore a twofold effect: an increase in salt marsh resilience in the short term but a net loss of sediment in the
349 long term that might jeopardize the entire intertidal system. If the marsh fails to keep up with SLR, large scale
350 marsh die-off might occur [*Morris et al.,* 2002; *Belliard et al.,* 2016]. Marsh drowning reduces tidal flow velocity in
351 the marsh channels, and limits the amount of sediments transported into the marsh interior, which in turn leads to
352 more marsh die-off [*Temmerman et al.,* 2012]. In this case, the trapping capacity of marsh channels will increase
353 because of a smaller *R,* further reducing the flux to the marshes.

354

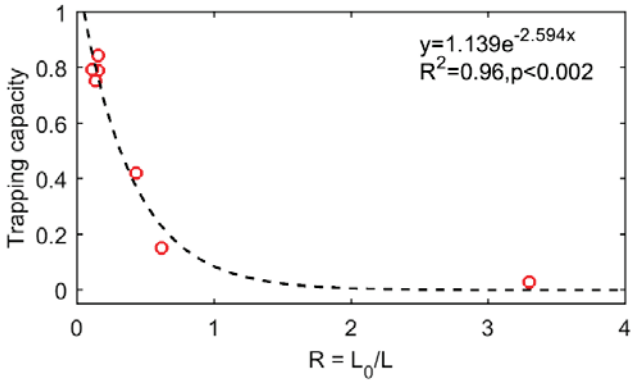


355

Figure 9. Relationships between sediment trapping capacity and the length ratio $R$ ($L_0/L$) of subdomains 1-7.

In both marsh-dominated and marsh-limited subdomains, only a small portion of sediments in the water column is transported into the marsh area. One possible reason is that our model does not account for wind waves and storms. *Mariotti et al.*, [2010] showed that a 15 m/s wind over the Virginia Coast produces bottom shear stresses comparable to tidal flow on tidal flats. More resuspension and longer permanence in the water column result in more deposition further into the marsh interior. Higher suspended sediment concentration within channels and in the sound ($C_0$ in equation 7) supplies more sediments to the marsh platform during flooding [*Lawson et al.*, 2007; *Mariotti et al.*, 2010]. Clearly, further quantitative analyses are essential to determine the effect of waves on sediment dynamics, although in our mesotidal study area the shear stress induced by wind waves is generally one order of magnitude smaller than the shear stress caused by tides [*Fagherazzi et al.*, 2014].

*Temmerman et al.*, [2003] empirically related sedimentation rates to time of tidal inundation, and distance to the nearest creek or marsh edge. However, sediment transport over the marsh platform is physically controlled by sediment properties and hydrodynamics, with the latter control less explored. Field measurements of flow within *Spartina alterniflora* canopies in North Carolina found a logarithmical decrease of mean velocity, total kinetic energy (TKE), and total suspended solid with distance, with 50% reduction of mean velocity and TKE within 5m of the marsh edge [*Leonard and Croft*, 2006]. Our model shows a similar trend: the velocity drops by approximately 50% within 300 m, and decreases further with distance (Fig.7B). *Leonard and Croft* [2006] also measured an abrupt increase of TKE when the mean velocity decreases at the marsh edge. In our model the sediment entering the marsh platform is perhaps underestimated because we do not account for the 3D turbulence structure of the flow, neglecting the possible wakes forming when the flow initially interacts with the vegetation at the marsh edge. In fact, the data of *Leonard and Croft* [2006] show that horizontal TKE dominates advection of sediment in the canopy, while vertical turbulence is of secondary importance [*Horstman et al.*, 2013; *Leonard and Croft*, 2006]. The concentration of sediment at the marsh edge and the decay rate determine the spatial distribution of deposition over the marsh platform. Comparing the regression plot based on model results with the simplified equation 8, we see that the maximum values of water depth and velocity during flood well capture the sediment transport over the marshes (Fig. 7C). This is because the maximum velocity $U_{max}$ controls sediment dynamics rather than the mean velocity [*Dyer,* 1995].

In Plum Island Sound, *Wilson et al*., [2014] attributed the increase in pond occurrence in recent decades to poor drainage density. Sparse channels are unable to bring sediment to the interior of the marsh, thus favoring pond formation and expansion. Lack of sediment inputs seem more important than waterlogging stress from SLR for pond dynamics [*Wilson et al*., 2014]. An increase in organic matter production and deposition could mitigate the lack of sediment inputs to the marsh interior. However, organic matter accounts for only 30% of the marsh soil in Plum Island Sound [*Hopkinson et al*., 2018]; thus it would be impossible to keep pace with SLR without the inorganic fraction. Similarly, *Mariotti* [2016] indicate that inorganic sediment deposition alone controls pond recovery using a simple numerical model. Our results are in agreement with this hypothesis. The low flow velocity on the marsh platform favors sediment deposition near the channels, to a distance of 100 m (Fig. 7c). Farther than that little deposition is present, favoring the formation of ponds, which indeed are on average 50 m away from channels (Fig. 8). We also note that finer resolution numerical models (~ 1 m) would be needed to capture the dynamics of narrow creeks and ditches dissecting the marsh surface. Ignoring these small-scale channels by using a mesh with a 20 m resolution could lead to an overestimation of the distance between marsh and channels.

## 5. Conclusions

Deposition of cohesive sediment within marshes not only provides nutrients for plant growth, but also builds land to counteract SLR. Strong friction in the vegetation canopy weakens the tidal flow thus facilitating sediment deposition. Cohesive sediments are typically transported in tidal channels and deposited on the marsh platform during high slack water. The spatial pattern of sedimentation differs for different grain sizes and settling velocities of cohesive sediments as a function of topography and marsh geometry. These patterns are very complex and can be hardly understood by field measurements. In this manuscript, we use a numerical model that solves the shallow water equations coupled to a vegetation module to study the fate of cohesive sediments within a marsh-dominated estuary. We test a series of scenarios, with different instants of sediment release, release in specific subdomains, and the role of sediment grain size. We determine how these scenarios affect the spatial distribution of sedimentation and sediment trapping capacity of the marshes.

Our main results are:

(1) Riverine sediments discharged in the bay during tidal flood will result in more sedimentation within the bay. Similarly, sediments mobilized by storm waves will be trapped in the system if the storm occurs during tidal flood, but partly exported to the ocean if the storm occurs during the ebb phase.

(2) Most sediment arriving in marsh-dominated areas is trapped there irrespectively of the tidal phase when the sediments was discharged by rivers or resuspended. Direct exchange of sediments between these areas is very limited. Sediment discharged from the tidal rivers deposit within the rivers themselves or in adjacent marshes.

(3) Trapping capacity of sediment in different intertidal subdomains decreases exponentially with $R$, the ratio between advection length and the typical spatial length of channels and tidal flats. Minor variations of $R$ result in large variations in trapping capacity of sediment. SLR, by increasing $R$, could considerably reduce sediment deposition in the system.

(4) Sediment deposition in the mash decreases exponentially with distance from the channels and marsh edge. The decay rate is a function of settling velocity and the maximum value of water depth and velocity on the marsh platform.

(5) Only a fraction of the sediments is deposited in the marshes, most sediment is deposited in shallow tidal flats and channels areas characterized by low flow. This is because sediments are unable to penetrate farther inside the marshes because of the limited water depths and velocities on the marsh platforms.

## Acknowledge

This research was funded by the National Science Foundation award DEB1237733 (VCR LTER) and the China Scholarship Council (201606140044).

## References

1. Baptist, M. J. (2005), Modelling floodplain biogeomorphology, TU Delft, Delft University of Technology.
2. Belliard, J. P., Di Marco, N., Carniello, L., & Toffolon, M. (2016). Sediment and vegetation spatial dynamics facing sea-level rise in microtidal salt marshes: Insights from an ecogeomorphic model. Advances in water resources, 93, 249-264.

3. Christiansen, T., P. L. Wiberg, and T. G. Milligan (2000), Flow and Sediment Transport on a Tidal Salt Marsh Surface, *Estuarine, Coastal and Shelf Science*, *50*(3), 315-331, doi:10.1006/ecss.2000.0548.
4. Correll, M. D., Hantson, W., Hodgman, T. P., Cline, B. B., Elphick, C. S., Shriver, W. G., ... & Olsen, B. J. (2018). Fine-Scale Mapping of Coastal Plant Communities in the Northeastern USA. Wetlands, 1-12.
5. Craft, C., Clough, J., Ehman, J., Joye, S., Park, R., Pennings, S., ... & Machmuller, M. (2009). Forecasting the effects of accelerated sea-level rise on tidal marsh ecosystem services. *Frontiers in Ecology and the Environment*, *7*(2), 73-78.
6. D'Alpaos, A., Lanzoni, S., Marani, M., & Rinaldo, A. (2007). Landscape evolution in tidal embayments: Modeling the interplay of erosion, sedimentation, and vegetation dynamics. Journal of Geophysical Research: Earth Surface, 112(F1).
7. Dai, Z., Liu, J. T., Wei, W., & Chen, J. (2014). Detection of the Three Gorges Dam influence on the Changjiang (Yangtze River) submerged delta. *Scientific Reports*, *4*, 6600.
8. Dai, Z., & Liu, J. T. (2013). Impacts of large dams on downstream fluvial sedimentation: an example of the Three Gorges Dam (TGD) on the Changjiang (Yangtze River). *Journal of Hydrology*, *480*, 10-18.
9. Dyer, K. R. (1995). Sediment transport processes in estuaries. In Developments in Sedimentology (Vol. 53, pp. 423-449). Elsevier.
10. Defne, Z., N. K. Ganju, and A. Aretxabaleta (2016), Estimating time-dependent connectivity in marine systems, *Geophysical Research Letters*, *43*(3), 1193-1201, doi:10.1002/2015gl066888.
11. Donatelli, C., Ganju, N.K., Fagherazzi, S. and Leonardi, N., 2018. SEAGRASSES IMPACT SEDIMENTS EXCHANGE BETWEEN TIDAL FLATS AND SALT MARSH, AND THE SEDIMENT BUDGET OF SHALLOW BAYS. Geophysical Research Letters.
12. Fagherazzi, et al. (2012), Numerical models of salt marsh evolution: Ecological, geomorphic, and climatic factors, *Reviews of Geophysics*, *50*(1), doi:10.1029/2011rg000359.
13. Fagherazzi, G. Mariotti, A. T. Banks, E. J. Morgan, and R. W. Fulweiler (2014), The relationships among hydrodynamics, sediment distribution, and chlorophyll in a mesotidal estuary, *Estuarine, Coastal and Shelf Science*, *144*, 54-64, doi:10.1016/j.ecss.2014.04.003.
14. Fagherazzi, G. Mariotti, P. Wiberg, and K. McGlathery (2013), Marsh Collapse Does Not Require Sea Level Rise, *Oceanography*, *26*(3), 70-77, doi:10.5670/oceanog.2013.47.
15. Fagherazzi, S., Bortoluzzi, A., Dietrich, W. E., Adami, A., Lanzoni, S., Marani, M., & Rinaldo, A. (1999). Tidal networks: 1. Automatic network extraction and preliminary scaling features from digital terrain maps. Water Resources Research, 35(12), 3891-3904.
16. Ganju, N. K., Kirwan, M. L., Dickhudt, P. J., Guntenspergen, G. R., Cahoon, D. R., & Kroeger, K. D. (2015). Sediment transport-based metrics of wetland stability. Geophysical Research Letters, 42(19), 7992-8000.
17. Ganju, Z. Defne, M. L. Kirwan, S. Fagherazzi, A. D'Alpaos, and L. Carniello (2017), Spatially integrative metrics reveal hidden vulnerability of microtidal salt marshes, *Nature communications*, *8*, ncomms14156.
18. Hopkinson, C. S., Morris, J. T., Fagherazzi, S., Wollheim, W. M., & Raymond, P. A. (2018). Lateral Marsh Edge Erosion as a Source of Sediments for Vertical Marsh Accretion. Journal of Geophysical Research: Biogeosciences.
19. Horstman, C. Dohmen-Janssen, and S. Hulscher (2013), Modeling tidal dynamics in a mangrove creek catchment in Delft3D.
20. Horstman, C. M. Dohmen-Janssen, T. J. Bouma, and S. J. M. H. Hulscher (2015), Tidal-scale flow routing and sedimentation in mangrove forests: Combining field data and numerical modelling, *Geomorphology*, *228*, 244-262, doi:10.1016/j.geomorph.2014.08.011.

21. Johnson, D. S., R. S. Warren, L. A. Deegan, and T. J. Mozdzer (2016), Saltmarsh plant responses to eutrophication, *Ecological Applications*, *26*(8), 2647-2659.
22. Kirwan, and A. B. Murray (2007), A coupled geomorphic and ecological model of tidal marsh evolution, *Proc Natl Acad Sci U S A*, *104*(15), 6118-6122, doi:10.1073/pnas.0700958104.
23. Kirwan, S. Temmerman, E. E. Skeehan, G. R. Guntenspergen, and S. Fagherazzi (2016), Overestimation of marsh vulnerability to sea level rise, *Nature Climate Change*, *6*(3), 253-260, doi:10.1038/nclimate2909.
24. Lawson, S., P. Wiberg, K. McGlathery, and D. Fugate (2007), Wind-driven sediment suspension controls light availability in a shallow coastal lagoon, *Estuaries and Coasts*, *30*(1), 102-112.
25. Leonard, and Croft (2006), The effect of standing biomass on flow velocity and turbulence in Spartina alterniflora canopies, *Estuarine, Coastal and Shelf Science*, *69*(3-4), 325-336, doi:10.1016/j.ecss.2006.05.004.
26. Leonard, L. A., and M. E. Luther (1995), Flow hydrodynamics in tidal marsh canopies, *Limnology and oceanography*, *40*(8), 1474-1484.
27. Leonardi, N., and S. Fagherazzi (2014), How waves shape salt marshes, *Geology*, *42*(10), 887-890, doi:10.1130/g35751.1.
28. Leonardi, N., Carnacina, I., Donatelli, C., Ganju, N.K., Plater, A.J., Schuerch, M. and Temmerman, S., 2017. Dynamic interactions between coastal storms and salt marshes: A review. Geomorphology.
29. Mariotti, G. (2016). Revisiting salt marsh resilience to sea level rise: Are ponds responsible for permanent land loss?. Journal of Geophysical Research: Earth Surface, 121(7), 1391-1407.
30. Mariotti, G., S. Fagherazzi, P. L. Wiberg, K. J. McGlathery, L. Carniello, and A. Defina (2010), Influence of storm surges and sea level on shallow tidal basin erosive processes, *Journal of Geophysical Research*, *115*(C11), doi:10.1029/2009jc005892.
31. Mehta, A. J. (2014), *An introduction to hydraulics of fine sediment transport*, World Scientific.
32. Mercier, C., and E. J. M. Delhez (2007), Diagnosis of the sediment transport in the Belgian Coastal Zone, *Estuarine, Coastal and Shelf Science*, *74*(4), 670-683, doi:10.1016/j.ecss.2007.05.010.
33. Morris, J. T., Sundareshwar, P. V., Nietch, C. T., Kjerfve, B., & Cahoon, D. R. (2002). Responses of coastal wetlands to rising sea level. Ecology, 83(10), 2869-2877.
34. Nardin, W., and D. A. Edmonds (2014), Optimum vegetation height and density for inorganic sedimentation in deltaic marshes, *Nature Geoscience*, *7*(10), 722-726, doi:10.1038/ngeo2233.
35. Nepf, H. M., and E. R. Vivoni (2000), Flow structure in depth-limited, vegetated flow, *Journal of Geophysical Research: Oceans*, *105*(C12), 28547-28557, doi:10.1029/2000jc900145.
36. Oorschot, M. v., M. Kleinhans, G. Geerling, and H. Middelkoop (2016), Distinct patterns of interaction between vegetation and morphodynamics, *Earth Surface Processes and Landforms*, *41*(6), 791-808, doi:10.1002/esp.3864.
37. Partheniades, E. (1965), Erosion and deposition of cohesive soils, Journal of the Hydraulics Division, 91(1), 105-139.
38. Ralston, D. K., and W. R. Geyer (2017), Sediment transport time scales and trapping efficiency in a tidal river, *Journal of Geophysical Research: Earth Surface*.
39. Reed, D. J., T. Spencer, A. L. Murray, J. R. French, and L. Leonard (1999), Marsh surface sediment deposition and the role of tidal creeks: implications for created and managed coastal marshes, *Journal of Coastal Conservation*, *5*(1), 81-90.
40. Syvitski, J. P., Vörösmarty, C. J., Kettner, A. J., & Green, P. (2005). Impact of humans on the flux of terrestrial sediment to the global coastal ocean. science, 308(5720), 376-380.
41. Syvitski, J. P., & Saito, Y. (2007). Morphodynamics of deltas under the influence of humans. Global and Planetary Change, 57(3-4), 261-282.

42. Tarandeep, S., K. Neil, and C. John (2017), Development of a coupled wave-flow-vegetation interaction model, *Computers and Geosciences*.
43. Temmerman, S., Moonen, P., Schoelynck, J., Govers, G., & Bouma, T. J. (2012). Impact of vegetation die-off on spatial flow patterns over a tidal marsh. Geophysical Research Letters, 39(3).
44. Temmerman, T. Bouma, G. Govers, and D. Lauwaet (2005a), Flow paths of water and sediment in a tidal marsh: Relations with marsh developmental stage and tidal inundation height, *Estuaries*, *28*(3), 338-352.
45. Temmerman, G. Govers, S. Wartel, and P. Meire (2003), Spatial and temporal factors controlling short-term sedimentation in a salt and freshwater tidal marsh, Scheldt estuary, Belgium, SW Netherlands, *Earth Surface Processes and Landforms*, *28*(7), 739-755.
46. Temmerman, S., T. J. Bouma, G. Govers, Z. B. Wang, M. B. De Vries, and P. M. J. Herman (2005b), Impact of vegetation on flow routing and sedimentation patterns: Three-dimensional modeling for a tidal marsh, *Journal of Geophysical Research: Earth Surface*, *110*(F4), n/a-n/a, doi:10.1029/2005jf000301.
47. Wiberg, P. L., J. A. Carr, I. Safak, and A. Anutaliya (2015), Quantifying the distribution and influence of non-uniform bed properties in shallow coastal bays, *Limnology and Oceanography: Methods*, *13*(12), 746-762, doi:10.1002/lom3.10063.
48. Wilson, C. A., Z. J. Hughes, D. M. FitzGerald, C. S. Hopkinson, V. Valentine, and A. S. Kolker (2014), Saltmarsh pool and tidal creek morphodynamics: Dynamic equilibrium of northern latitude saltmarshes?, *Geomorphology*, *213*, 99-115.
49. Yang, J. Q., F. Kerger, and H. M. Nepf (2015), Estimation of the bed shear stress in vegetated and bare channels with smooth beds, *Water Resources Research*, *51*(5), 3647-3663, doi:10.1002/2014wr016042.
50. Zhao, L., C. Chen, J. Vallino, C. Hopkinson, R. C. Beardsley, H. Lin, and J. Lerczak (2010), Wetland-estuarine-shelf interactions in the Plum Island Sound and Merrimack River in the Massachusetts coast, *Journal of Geophysical Research*, *115*(C10), doi:10.1029/2009jc006085.